CMS Physics Analysis Summary

Contact: cms-pag-conveners-susy@cern.ch 2011/03/23

Inclusive search for squarks and gluinos at $\sqrt{s} = 7$ TeV

The CMS Collaboration

Abstract

A search is performed for heavy particle pairs produced in $\sqrt{s} = 7$ TeV proton-proton collisions with 35 pb^{-1} of data collected by the CMS detector in 2010 at the CERN Large Hadron Collider. The search is sensitive to generic SUSY models provided superpartner particles are kinematically accessible, with minimal assumptions on properties of the Lightest Superpartner Particle (LSP). The baseline selection is inclusive requiring only two or more reconstructed jets. The kinematic consistency of the selected events is tested against the hypothesis of heavy particle pair production using the dimensionless razor (R) variable. The new physics signal is characterized by a broad peak in the distribution of M_R, where M_R is an event-by-event indicator of the heavy particle scale. After data-based background modeling and background rejection based on R and M_R no significant excess of events is found beyond the Standard Model expectations. The results are interpreted in the context of the Constrained Minimal Supersymmetric Standard Model (CMSSM).

1 Introduction

Experimental limits from the Tevatron and LEP showed that superpartner particles, if they exist, are significantly heavier than their Standard Model counterparts. Thus proposed experimental searches for R-parity conserving supersymmetry (SUSY) [1–5] at the LHC have focused on a combination of two SUSY signatures: multiple energetic jets and/or leptons from the decays of pair-produced superpartners, and large missing transverse energy (E_T^{miss}) from the two lightest superpartners (LSPs) produced in those same decay chains.

In this note we present a new approach that is inclusive both for SUSY and in the larger context of physics beyond the Standard Model. The starting point for this novel "razor" [6] analysis is that we are interested in the production of pairs of heavy particles (of which gluinos and squarks are examples), whose masses are significantly larger than those of any Standard Model particle. The analysis is designed to discriminate heavy pair production kinematically from Standard Model backgrounds, without making strong assumptions about the E_T^{miss} spectrum or any details of the subsequent decay chains. The baseline selection requires two or more reconstructed objects in the final state, which can be any combination of calorimetric jets as well as electrons and muons satisfying lepton selection criteria. These objects are grouped into two "mega-jets". The razor analysis tests the consistency, event by event, of the hypothesis that the two mega-jets represent the visible portion of the decays of two heavy particles. This strategy is complementary to canonical searches for signals in the tails of the E_T^{miss} distribution.

2 The CMS detector

A detailed description of the Compact Muon Solenoid (CMS) detector can be found elsewhere [7]. CMS uses a right-handed coordinate system, with the origin located at the nominal collision point, the x-axis pointing towards the center of the LHC, the y-axis pointing up (perpendicular to the LHC plane), and the z-axis along the (anti-clockwise) beam direction. The azimuthal angle ϕ is measured with respect to the x axis in the xy plane and the polar angle θ is defined with respect to the z axis. The pseudorapidity is $\eta = -\ln(\tan(\theta/2))$.

A characteristic feature of the CMS detector is its superconducting solenoid magnet, of 6 m internal diameter, providing a field of 3.8 T. Within the field volume are the silicon pixel and strip tracker, the crystal electromagnetic calorimeter (ECAL) and the brass/scintillator hadron calorimeter (HCAL). Muons are measured in gas-ionization detectors embedded in the steel return yoke. The ECAL has energy resolution of better than 0.5 % above 100 GeV. The HCAL, when combined with the ECAL, measures jets with a resolution $\Delta E/E \approx 100\,\%/\sqrt{E} \oplus 5\,\%$.

3 The razor analysis

A generic SUSY-like signal is the pair production of two heavy particles each decaying to an unseen LSP plus jets. Using the idea of event hemispheres [8], we can treat all the ≥ 2 jets final states by combining all reconstructed jet objects in each hemisphere into a single "mega-jet". Thus in terms of mega-jets all events are forced into a dijet-like topology. To the extent that the pair of mega-jets accurately reconstruct the visible portion of the underlying parent particle decays, the signal kinematics is equivalent to pair production of two heavy squarks (without loss of generality) $\tilde{q}_1$, $\tilde{q}_2$, with $\tilde{q}_i \to \mathrm{j_i}\tilde{\chi}_i^0$, where the $\tilde{\chi}$'s are LSPs (or Next-to-LSPs if these particles are weakly interacting and escape the detector) and j_i denotes the visible products of the decays. In the approximation that the heavy squarks are produced at threshold, the center of

mass (CM) frame kinematics are simply

$$p_{j1} = \frac{M_\Delta}{2}(1, \hat{u_1}) \ , \quad p_{j2} = \frac{M_\Delta}{2}(1, \hat{u_2}) \ , \tag{1}$$

$$p_{\chi_1} = \frac{M_\Delta}{2}(\frac{2M_{\tilde{q}}}{M_\Delta} - 1, -\hat{u_1}) \ , \quad p_{\chi_2} = \frac{M_\Delta}{2}(\frac{2M_{\tilde{q}}}{M_\Delta} - 1, -\hat{u_2}) \ , \tag{2}$$

where $\hat{u_i}$ are unit vectors and

$$M_\Delta \equiv \frac{M_{\tilde{q}}^2 - M_{\tilde{\chi}}^2}{M_{\tilde{q}}} \ . \tag{3}$$

An event by event approximate reconstruction is made assuming the dijet signal topology. In this approximation the "R frame" [6] would be the CM frame for signal events, if the squarks were produced at threshold and if the CM system had no overall transverse momentum from initial state radiation (ISR). The R frame is the longitudinally boosted frame that equalizes the magnitude of the two mega-jet 3-momenta. This longitudinal boost is defined by

$$\beta_R \equiv \frac{E^{j1} - E^{j2}}{p_z^{j1} - p_z^{j2}} \ , \tag{4}$$

where E^{j1}, E^{j2} and p_z^{j1}, p_z^{j1} are the mega-jet energies and longitudinal momenta respectively. To the extent that the R-frame matches the true CM frame, the simple kinematics indicate that for the signal events the maximum value of the scalar sum of the mega-jets transverse momenta (p_T^1, p_T^2) is M_Δ. The maximum value of the E_T^{miss} is also M_Δ. We define a transverse variable whose maximum value for signal events in the same limit is also M_Δ:

$$M_T^R \equiv \sqrt{\frac{|E_T^{miss}|(p_T^{j1} + p_T^{j2}) - \vec{E}_T^{miss} \cdot (\vec{p}_T^{\,j1} + \vec{p}_T^{\,j2})}{2}} \ . \tag{5}$$

Signal events are characterized by the heavy scale M_Δ, while backgrounds are not. The event-by-event estimator of M_Δ is

$$M_R \equiv 2|\vec{p}_{\rm j1}^{\,R}| = 2|\vec{p}_{\rm j2}^{\,R}| = 2\sqrt{\frac{(E^{j1}p_z^{j2} - E^{j2}p_z^{j1})^2}{(p_z^{j1} - p_z^{j2})^2 - (E^{j1} - E^{j2})^2}} \ , \tag{6}$$

where $\vec{p}_{\rm j1}^{\,R}$ and $\vec{p}_{\rm j2}^{\,R}$ are the 3-momenta of the mega-jets in the R frame. For signal events in the limit where the R frame and the true CM frame coincide M_R equals M_Δ, and more generally M_R is expected to peak around M_Δ for signal events [6]. For QCD dijet and multijet events the only relevant scale is $\sqrt{\hat{s}}$. Qualitatively we expect M_R to peak for the signal over a steeply falling background. Thus the search for an excess of signal events in a tail of a distribution is recast as a search for a peak on top of a steeply falling Standard Model residual tail. To extract the peaking signal we need first to reduce the QCD multijet background to manageable levels. This is achieved using the "razor" variable defined as

$$R \equiv \frac{M_T^R}{M_R} \ . \tag{7}$$

Recall that for signal events M_T^R has a maximum value of M_Δ (i.e. a kinematic edge); thus R has a maximum value of approximately 1 and the distribution of R for signal peaks around 0.5. These properties motivate the appropriate kinematic requirements for the signal selection and background reduction. We note that, while M_T^R and M_R measure the same scale (one as an end-point the other as a peak), they are largely uncorrelated for signal events as shown in Figure 1.

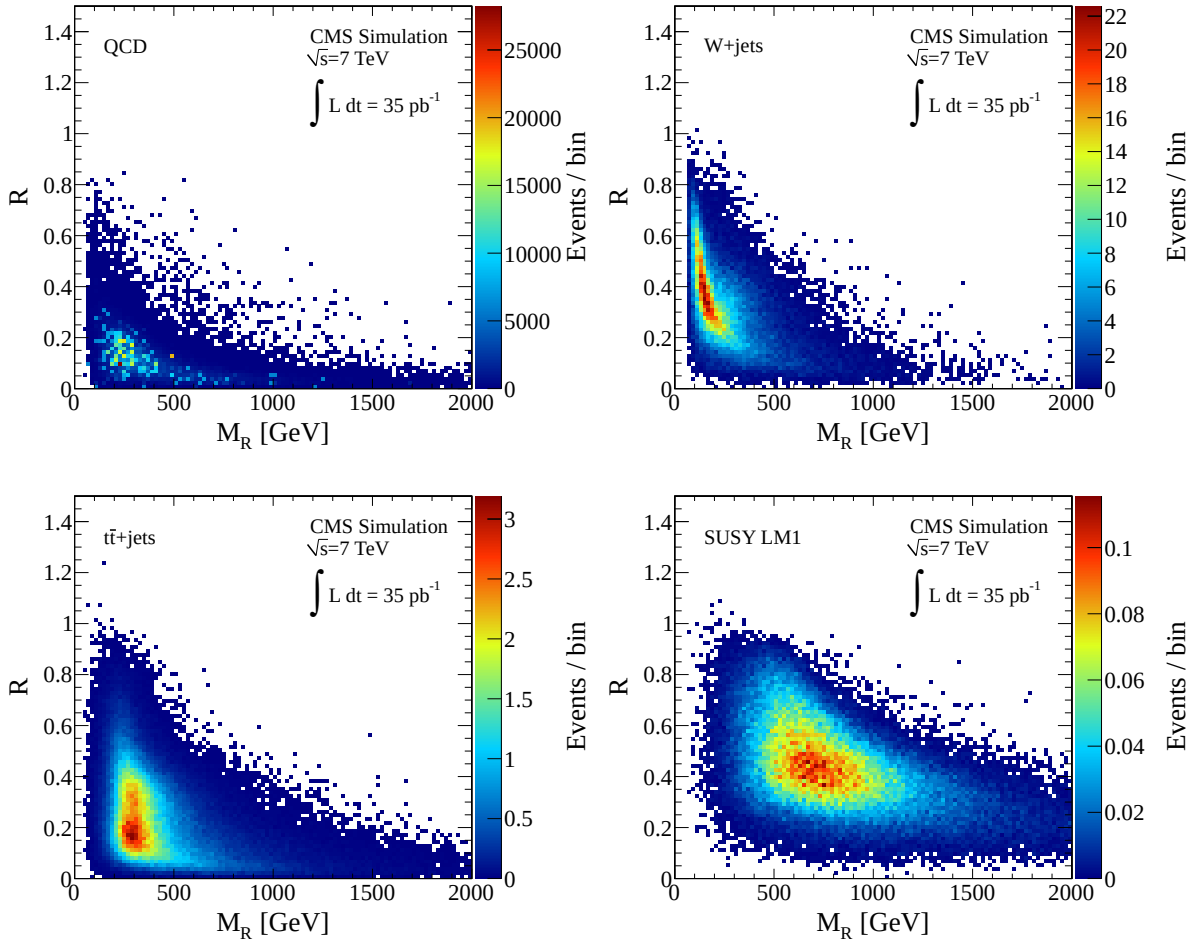

Figure 1: The razor plane: M_R versus R yields for 10 pb^{-1} Monte Carlo simulated samples: QCD multijets (top left), W+jets (top right), t+X (bottom left) and a CMS SUSY benchmark model (LM1 [8]) with $M_\Delta = 597$ GeV.

3.1 Analysis Path

In this analysis the Standard Model background shapes and normalizations are obtained from the data. The backgrounds are extracted from control regions in the razor variables R and M_R where the Standard Model processes dominate and are well described. The background in these regions is synthesized from the simulated individual background components and validated for shape and normalization with the data observed in these control regions. The analysis flow is as follows:

1. A baseline kinematic selection is defined using the mega-jets.
2. Inclusive data sets are used collected using the electron, muon or hadronic jet CMS triggers.
3. These data sets are queried for the presence of a well-identified electron or muon. Based on the presence or absence of such a lepton the event is moved to one of three disjoint event samples referred to as the electron, muon and hadronic "boxes". These boxes serve as controls of processes in the Standard Model with leptons, jets and neutrinos, i.e., QCD

multijets, W or Z+jets, t+X, and dibosons. The large R and high M_R regions of these boxes are not used for the background estimates but instead constitute signal candidate regions.

4. In the electron box, electrons are clustered with jets in the definition of the mega-jet hemispheres. Jets matched to these electrons are removed to avoid double-counting. In the muon box, muons are added to the jet list and included in the mega-jet clustering.

5. Events remaining in the hadronic box primarily consist of QCD multijets, $Z \to \nu\bar{\nu}$, $W \to \ell\nu$+jets and top events in ℓ+jets+E_T^{miss} final states with charged leptons that did not satisfy the electron or muon selections. The shapes and normalizations of the non-QCD background processes in the hadronic box are determined from the control lepton boxes in appropriate regions in the R, M_R plane. The properties of M_R as a function of R minimize the signal contamination in the Standard Model normalization.

6. The QCD background shape and normalization in either of the lepton boxes is extracted by reversing the lepton isolation requirements to obtain control samples dominated by QCD. The QCD shape in the hadronic box is obtained using prescaled QCD control samples, while the normalization is floated in a fit that takes into account the turn-on curves of the triggers used.

7. Having determined the R and M_R shape and normalization of the backgrounds in the control regions, the Standard Model yields are predicted in the large R and high M_R event sample for each box.

4 Event Selection

The analysis uses only data sets for which the CMS detector was declared fully operational in nominal collider and detector conditions. The relevant data sets are recorded using triggers based on electron, muons, and H_T, the uncorrected scalar sum of the transverse energy of jets reconstructed at the trigger level. Prescaled jet triggers with low thresholds are used to demonstrate and validate the QCD multijet background estimation in the hadronic box.

Events are required to have at least one good reconstructed interaction vertex [9]. When multiple vertices are found, the one with the highest associated $\sum_{track} p_T$ is used.

Jets are reconstructed offline using calorimeter energy deposits clustered using the infrared-safe anti-k_T [10] algorithm with a cone size $R_{\text{cone}} = 0.5$ in $(\eta \times \phi)$ space. Jets are corrected for calorimetric energy response and η non-uniformity using Monte Carlo derived corrections and are required to have $p_T > 30$ GeV/c and $|\eta| < 3.0$. The jet energy scale uncertainty for these corrected jets is 5% [11]. E_T^{miss} is reconstructed using the CMS Particle Flow algorithm [12].

The electron and muon reconstruction and identification criteria are described in Reference [13]. Electrons and muons are required to have p_T>20 GeV/c and be within $|\eta| < 2.5$ and 2.1 respectively.

If an event has at least two jets we form two hemispheres. The hemisphere algorithm used is taken from [8]; it selects the jet combination minimizing the invariant masses of the two mega-jets in the R frame. We form all the possible combinations of jets into two groups so that at least one jet is present in each group. The jets in each hemisphere are combined into mega-jets by adding their four-momenta.

After the construction of the two mega-jets the boost variable $|\beta_R|$ is computed; due to the approximations mentioned above, β_R can fall in an unphysical region (≥ 1) for signal or background events; these events are removed. The additional requirement $|\beta_R| \leq 0.99$ is imposed to remove events for which the razor variables become singular. The azimuthal angular difference between the mega-jets is required to be < 2.8 radians; this requirement suppresses nearly back-to-back QCD dijet events. These requirements define the analysis inclusive baseline selection. After this selection the signal efficiency in the CMSSM [14–17] parameter space for gluino mass ~ 600 GeV/c^2 is over 50%.

5 Background Estimation

5.1 QCD multijets

The QCD multijet control box is defined from event samples recorded with the prescaled jet triggers passing the baseline analysis selection for events without a well-identified isolated electron or muon. The trigger requires at least two jets with average uncorrected $p_T > 15$ GeV/c. The low jet threshold assures that QCD multijets dominate this sample for low M_R thus allowing the extraction of the M_R, R distribution shapes for QCD multijet events.

The M_R distributions for events satisfying the QCD control box selection, for different values of the R cut, are shown in Fig. 2 (left, center). The M_R distribution is exponentially falling, after a turn-on at low M_R resulting from the p_T threshold requirement on the jets entering the mega-jet calculation. The exponential region of these distributions is fitted for each value of R to extract the slope, denoted by S. The value of S which maximizes the likelihood in the exponential fit is found to be linear function of R^2. Fitting S as a function of R^2 with a first order polynomial $S = a + bR^2$ determines the values of a and b as shown in Fig. 2 (right).

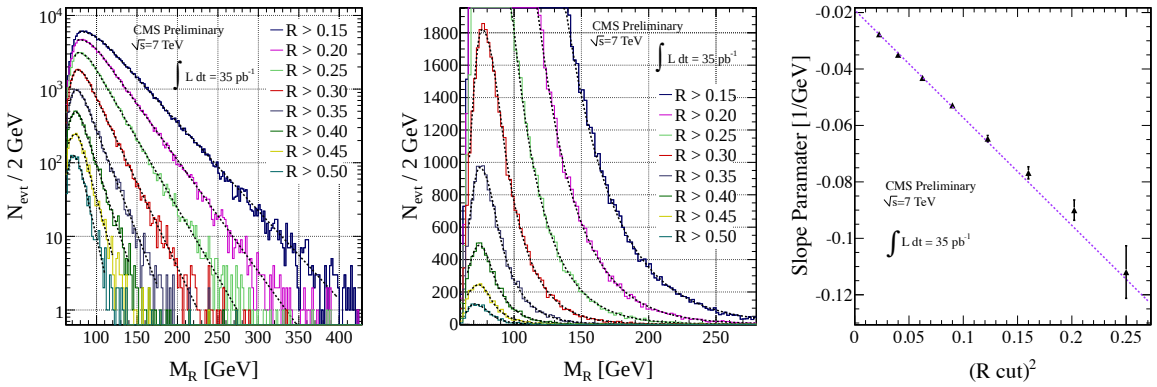

Figure 2: (left and center) M_R distributions for different values of the R threshold for events in data selected in the QCD control box. Fits to the exponential part of the M_R distribution are shown as dotted black lines. (right) The exponential slope S from fits to the M_R distribution, as a function of the R threshold for data events in the QCD control box.

When measuring the exponential slopes of the M_R distributions as a function of the R threshold, the correlations due to common events are neglected. The effect of these correlations is studied by using pseudo-experiments and is found to be negligible. To measure the shape of the QCD component in the lepton boxes the corresponding lepton trigger data sets are used with the baseline selection and reversed lepton isolation criteria.

The R threshold shapes the M_R distribution in a simple thus predictable way. Event selections with combined R and M_R thresholds are found to suppress jet mis-measurements, including catastrophic mis-measurements of the electromagnetic or hadronic component of a jet's energy, or other anomalous calorimetric noise signals [18], [19].

5.2 W+jets, Z+jets and top+X backgrounds

Using the muon (MU) control box, M_R intervals for different R thresholds are identified where the data samples are dominated by $W(\mu\nu)$+jets events. In both Monte Carlo simulated events and the data, the M_R distribution is well described with two independent exponential components, simultaneously floating both slopes along with their relative and absolute normalizations as shown in Fig. 3 (left). The slope parameters characterizing the exponential behavior of the 1^{st} $W(\ell\nu)$+jets component are also shown in Fig. 3 (right). The values of the parameters a and b that describe the R^2 dependence of the slope are in good agreement with the values extracted from simulated $W(\mu\nu)$+jets events. The ratios $\rho^{\mathrm{DATA/MC}}$ of the values of the slope parameters a and b measured in the data to those predicted from simulated events are taken as correction factors used to predict the shapes of other electroweak background components in the boxes. The results of the two component exponential fit for $W(e\nu)$+jets events in the electron (ELE) box , along with the extracted 1^{st} component slope parameters are shown in Fig. 4.

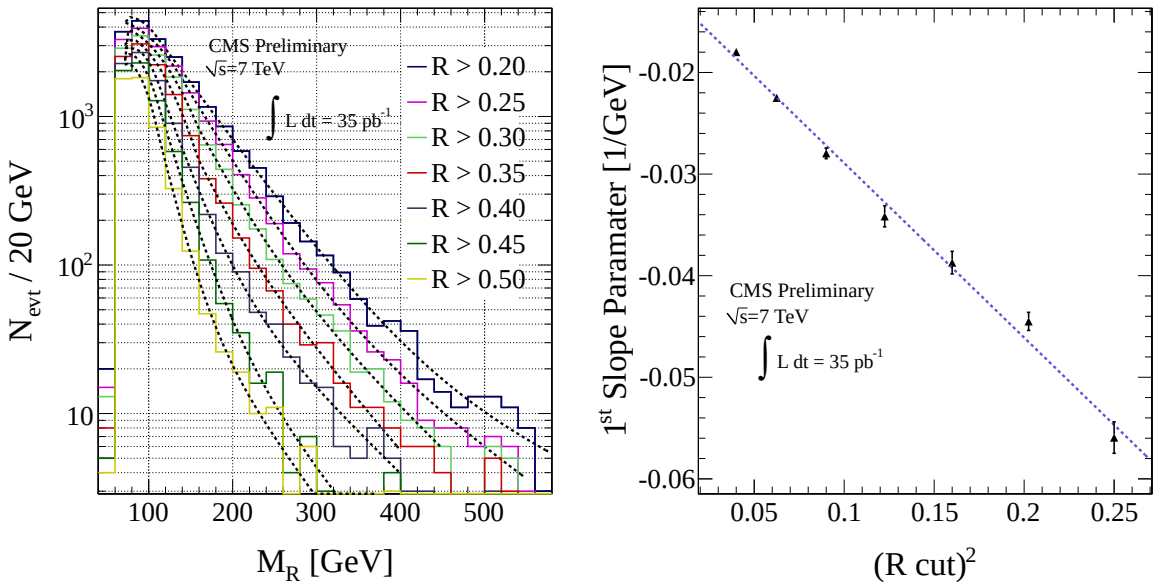

Figure 3: (left) M_R distributions for different values of the R threshold for events in data selected in the MU box. The dotted colored lines show two independent exponential components fit to the the M_R distribution. (right) Value of the first exponential slope S from fits to the M_R distribution, as a function of the R threshold for data events in the MU box.

The ratios $\rho^{\mathrm{DATA/MC}}$ measured in the MU and ELE boxes for the 1^{st} component slope are

$$\rho(a)^{\mathrm{DATA/MC}}_{MU} = \frac{117 \pm 3}{126 \pm 3} = 0.93 \pm 0.03 \;\; ; \;\; \rho(b)^{\mathrm{DATA/MC}}_{MU} = \frac{172 \pm 4}{171 \pm 4} = 1.00 \pm 0.03 \tag{8}$$

$$\rho(a)^{\mathrm{DATA/MC}}_{ELE} = \frac{125 \pm 3}{124 \pm 3} = 1.00 \pm 0.03 \;\; ; \;\; \rho(b)^{\mathrm{DATA/MC}}_{ELE} = \frac{176 \pm 4}{189 \pm 4} = 0.93 \pm 0.03 \tag{9}$$

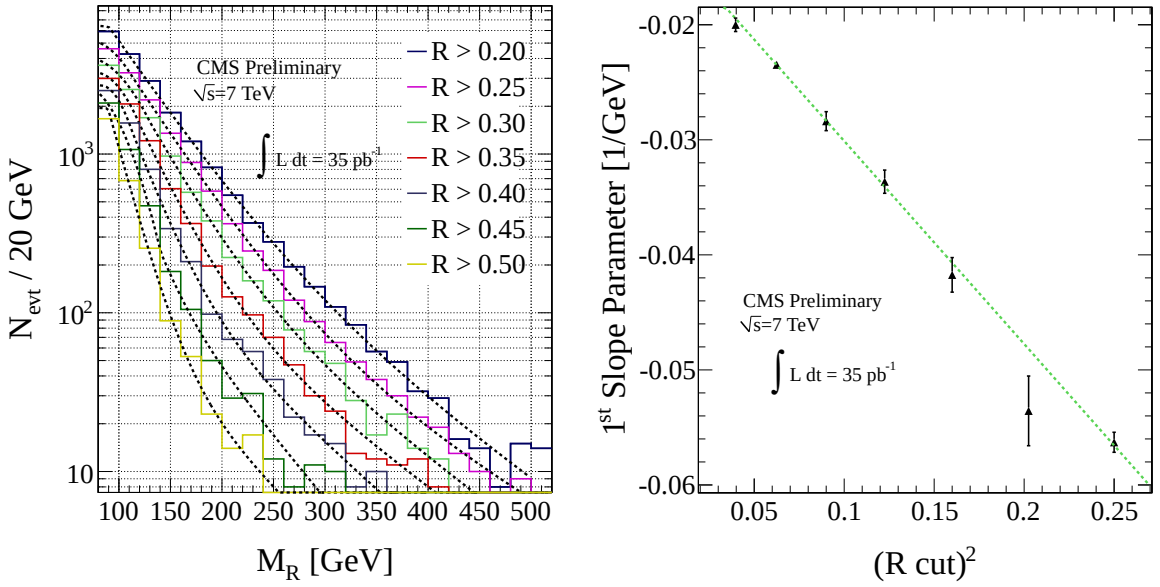

Figure 4: (left) M_R distributions for different values of the R threshold for events in data selected in the ELE box. The dotted colored lines show two independent exponential components fit to the the M_R distribution. (right) Value of the first exponential slope S from fits to the M_R distribution, as a function of the R threshold for data events in the ELE box.

The DATA/MC correction factors measured independently in the MU and ELE boxes are combined, yielding:

$$\rho(a)_1^{\mathrm{DATA/MC}} = 0.97 \pm 0.02 \;\; ; \;\; \rho(b)_1^{\mathrm{DATA/MC}} = 0.97 \pm 0.02 \tag{10}$$

These factors are used to correct the slope parameters measured in simulated events for each of the background processes appearing in the MU, ELE and hadronic (HAD) boxes. The relative normalizations of the W/Z+jets components are determined using the relevant cross section ratios as measured in data.

For the $Z(\nu\nu)$+jets component in the HAD box the DATA/MC correction factors are measured using a "lepton-as-neutrino" view of leptonic events, where the electron and muon are excluded from the mega-jet reconstruction kinematically mimicking the presence of an additional neutrino. Both in the data and in Monte Carlo simulated events there is only one exponential component observed for $W(\ell\nu)$+jets in the lepton-as-neutrino treatment of the ELE and MU boxes, which is found to agree with the $W(\ell\nu)$+jets second component slope in the default treatment. The first component of the $W(\ell\nu)$+jets in the default treatment corresponds to events where the electron or muon significantly contribute in the mega-jet reconstruction and is therefore absent in the lepton-as-neutrino treatment.

The slope of the second component of the $W(\ell\nu)$+jets is measured using the lepton-as-neutrino treatment of the ELE and MU boxes. The combined DATA/MC correction factors measured for the 2^{nd} $W(\ell\nu)$+jets component and used for the $Z(\nu\nu)$+jets and t+X events are:

$$\rho(a)_2^{\mathrm{DATA/MC}} = \frac{96 \pm 2}{95 \pm 1} = 1.01 \pm 0.02 \;\; ; \;\; \rho(b)_2^{\mathrm{DATA/MC}} = \frac{29 \pm 2}{31 \pm 1} = 0.94 \pm 0.07 \tag{11}$$

For the final background prediction the magnitude of the relative normalization between the

two $W(\ell\nu)$+jets components, denoted f^W, is floated and is determined through a binned likelihood fit in the region $200 < M_R < 400$ GeV.

6 Results

6.1 Lepton box background predictions

The W+jets and Z+jets background M_R shapes use as a normalization reference the W and Z cross-sections, with corresponding uncertainties, as measured in electron and muon final states [13]. The $t\bar{t}$ cross section [20] is also used from the CMS measurement in the dilepton channel to normalize the M_R shape of the $t\bar{t}$+jets background. The measured values of these cross sections are summarized below:

$$\sigma(pp \to WX) \times \mathrm{BF}(W \to \ell\nu) = 9.951 \pm 0.073(\mathrm{stat}) \pm 0.280(\mathrm{syst}) \pm 1.095(\mathrm{lum})\ \mathrm{nb} \quad (12)$$

$$\sigma(pp \to ZX) \times \mathrm{BF}(Z \to \ell\ell) = 0.931 \pm 0.026(\mathrm{stat}) \pm 0.023(\mathrm{syst}) \pm 0.102(\mathrm{lum})\ \mathrm{nb} \quad (13)$$

$$\sigma(pp \to t\bar{t}) = 194 \pm 72(\mathrm{stat}) \pm 24(\mathrm{syst}) \pm 21(\mathrm{lum})\ \mathrm{pb}\ . \quad (14)$$

These cross sections are used to fix the relative ratio of the W/Z+jets and t+X backgrounds. The region [125$< M_R <$ 175] GeV where the QCD contribution is negligible and the $W(\ell\nu)$+jets component is dominant is used to set the overall normalization factor of the total background prediction.

The final background prediction in the ELE and MU boxes for $R > 0.45$ is shown in Fig. 5. The

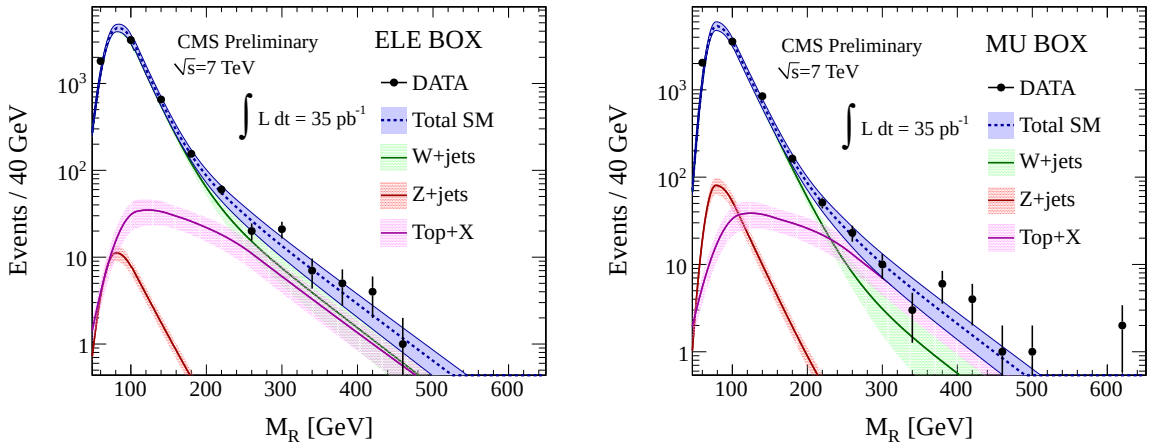

Figure 5: Background predictions for the M_R distribution in the the ELE (left) and MU (right) boxes with $R > 0.45$ compared with the data.

integrated yields for M_R>500 in the data, with the corresponding predictions, are summarized in Table 1. We observe general agreement between the predicted and observed yields. The p-value of the measurement in the MU box given the predicted background (with its uncertainties) and the observed number of events is 0.1. A summary of the uncertainties entering the background measurements is presented in Table 2.

Table 1: Predicted and observed yields for ELE and MU box for R >0.45 and M_R>500 GeV.

R (0.45) / M_R (500)	Predicted	Observed
ELE box	0.63 ± 0.23	0
MU box	0.51 ± 0.20	3

Table 2: Summary of uncertainties entering the background predictions for the MU and ELE boxes. The range in the Monte Carlo uncertainties is due to the different Monte Carlo statistics of the different background component samples.

Parameter	Description	Relative Magnitude
Slope parameter a	systematic bias from correlations in fits	5%
Slope parameter b	systematic bias from correlations in fits	10%
Slope parameter a	uncertainty from Monte Carlo	1-10%
Slope parameter b	uncertainty from Monte Carlo	1-10%
$\rho(a)^{\mathrm{DATA/MC}}$	measured from DATA	3%
$\rho(b)^{\mathrm{DATA/MC}}$	measured from DATA	3%
Normalization	systematic+statistical component	3-8%
f^W	extracted in MLFit (W only)	30%
$W/t\bar{t}$ cross-section ratio	CMS measurements (top only)	40%
W/Z cross-section ratio	CMS measurements (Z only)	19%

6.2 Hadronic box background predictions

The procedure for assembling the total background predictions in the hadronic box is summarized as follows:

- Construct the background shapes in M_R using measured values of a and b from simulated events, with data-driven correction factors applied and taking into account the H_T trigger turn-on efficiency.
- Set the relative normalizations of the W/Z+jets and t+X backgrounds using relevant inclusive cross-section measurements from CMS [13, 20].
- Set the overall normalization by measuring the event yields in the lepton boxes, corrected for lepton reconstruction and identification.
- With the shapes and normalizations of the backgrounds fixed, determine the normalization of the QCD background from a fit to the low M_R region.

The kinematic similarities among background events falling in different physics object boxes are exploited by measuring normalizations in the lepton boxes in regions of phase-space (with respect to the variables R and M_R) that are nearly identical for the different boxes. As a result, any systematic shortcomings in the Monte Carlo simulation description of R or M_R acceptance efficiencies or values of the exponential slope parameters are accounted for in the normalization procedure through DATA/MC correction factors derived in similar regions of kinematic phase-space.

With all background normalizations and shapes fixed the final hadronic box background prediction follows from a binned likelihood fit of the total background shape to the data in the interval $80 < M_R < 400$ GeV, where parameters related to the H_T trigger turn-on shapes as well as f^w and the overall normalization of the QCD background are simultaneously floated. A set of pseudo-experiments is used to test the overall fit for coverage of the various floated parameters and for systematic biases. A 2% systematic uncertainty is assigned to the high M_R

background prediction that encapsulates systematic effects related to the fit procedure. Fig. 6 shows the final hadronic box background predictions with all uncertainties on this prediction included for $R > 0.5$. The observed M_R yield is consistent with the predicted one over the entire M_R range. The predicted and observed background yields in the high M_R region are summarized in Table 3. A summary of the uncertainties entering these background predictions is listed in Table 4. A larger R requirement is used in the HAD box due to the larger background.

Table 3: Predicted and observed yields for M_R>500 GeV with $R > 0.5$ in the HAD Box.

M_R cut	Predicted	Observed
$M_R > 500$ GeV	5.5 ± 1.4	7

Table 4: Summary of uncertainties entering the background predictions for the HAD Box.

Parameter	Description	Relative Magnitude
Slope parameter a	systematic bias from correlations in fits	5%
Slope parameter b	systematic bias from correlations in fits	10%
Slope parameter a	uncertainty from Monte Carlo	1-10%
Slope parameter b	uncertainty from Monte Carlo	1-10%
$\rho(a)^{\mathrm{DATA/MC}}$	measured from DATA	3%
$\rho(b)^{\mathrm{DATA/MC}}$	measured from DATA	3%
Normalization	systematic+statistical component	8%
Trigger Parameters	systematic from fit toys	2%
f^W	extracted in MLFit (W only)	13%
$W/t\bar{t}$ cross-section ratio	CMS measurements (top only)	40%
W/Z cross-section ratio	CMS measurements (Z only)	19%

7 Limits in the CMSSM parameter space

The likelihood for the number of observed events n is modeled as a Poisson function, given the sum of the signal s and the background b. A posterior probability density function for the signal yield is derived using Bayes theorem, assuming a flat prior for the signal and a log-normal prior for the background.

A 95% probability model independent upper limit is derived by integrating the posterior probability distribution function between 0 and s^* so that $\int_0^{s^*} P(s)ds = 0.95 \int_0^{\infty} P(s)ds$. The observed limit in the hadronic box is $s < 8.4$ (expected 7.2 ± 2.7); in the muon box $s < 6.3$ (expected 3.5 ± 1.1); and in the electron box $s < 2.9$ (expected 3.6 ± 1.1). For 10% of the pseudo-experiments in the muon box the expected limit is worse than the observed. The stability of the result was studied against different choices of the prior. In particular, using the reference posterior derived as in Ref. [21] the limit in the hadronic box is $s < 8.0$, in the muon box $s < 5.3$, and in the electron box $s < 2.9$.

The limit is projected on the m_0 and $m_{1/2}$ plane comparing it with the predicted yield and excluding the model if $s(m_0, m_{1/2}) > s^*$. The systematic uncertainty on the signal yield (coming from the uncertainty on the luminosity, the selection efficiency, and the theoretical uncertainty associated to the cross section calculation) is modeled according to a Gaussian prior. The uncertainty on the selection efficiency includes the effect of jet-energy-scale corrections, parton distribution function (PDF) uncertainties (following [22]), and the description of initial state

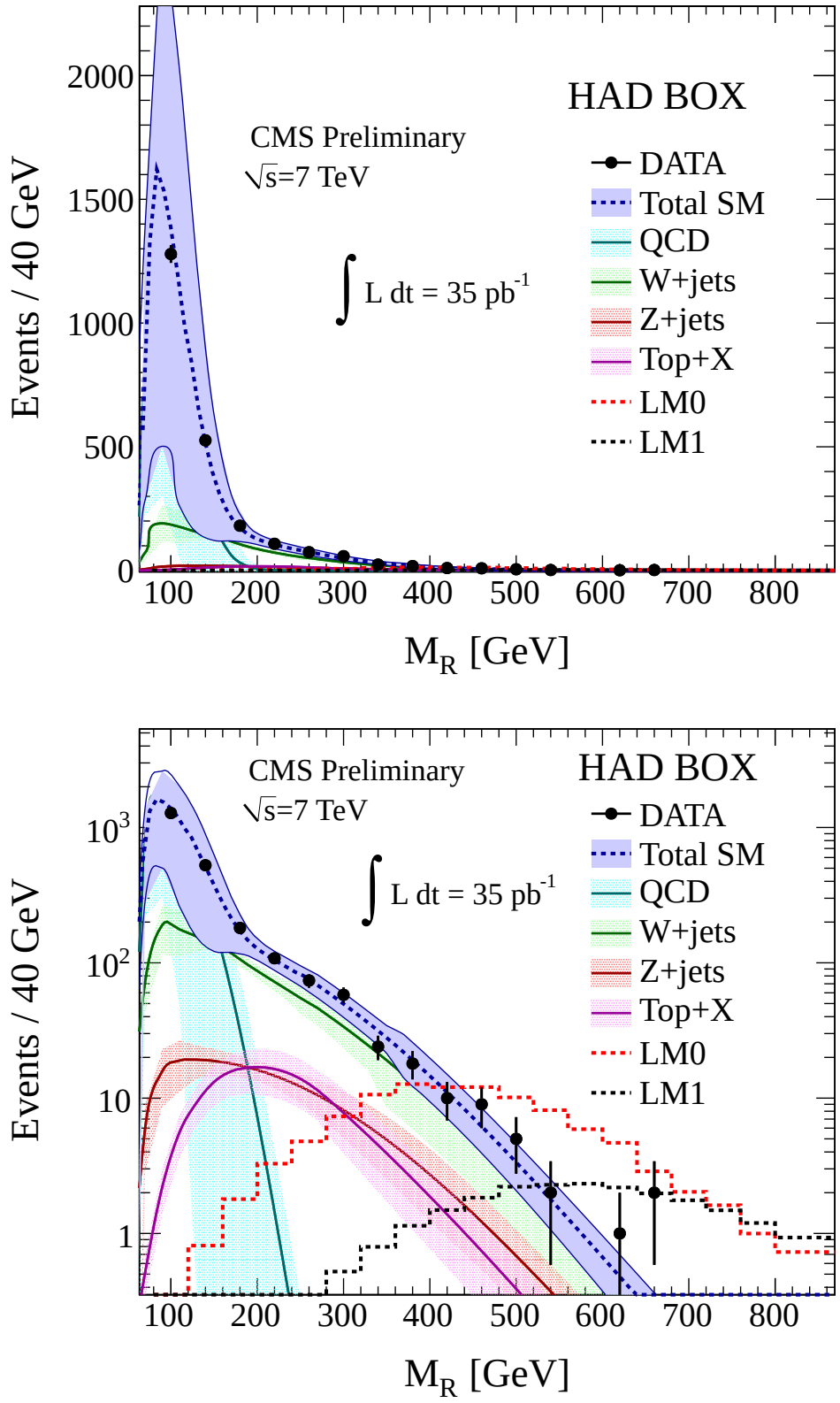

Figure 6: Final background prediction for the HAD Box with $R > 0.5$ linear scale (left) and $R > 0.5$ log scale (right).

radiation. All the effects are summed in quadrature to obtain the value of the σ parameter of the Gaussian as shown in table 5.

Table 5: Breakdown and total systematic uncertainties on the signal yield. For the CMSSM scan the NLO cross section uncertainty is included.

box	MU	ELE	HAD
Experiment			
JES	1%	1%	1%
Data/MC ϵ	6%	6%	6%
$\mathcal{L}$[23]	4%	4%	4%
Theory			
ISR	1%	1%	0.5%
PDF	3-6%	3-6%	3-6%
Total	8-9%	8-9%	8-9%
CMSSM			
NLO σ	16-18%	16-18%	16-18%
Total	17-19%	17-19%	17-19%

The result is shown in Figures 7–9 in the CMSSM $m_0/m_{1/2}$ plane for ($\tan\beta = 3$, $A_0 = 0$, sgnμ = +) together with the 68% probability band for the expected limit, obtained applying the same procedure to an ensemble of background-only Monte Carlo pseudo-experiments. The band is computed around the median of the limit distribution. The limit is also shown in Figures 10–12 in the CMSSM $m_0/m_{1/2}$ plane for ($\tan\beta = 10$, $A_0 = 0$, sgnμ = +). In Figures 13, 14 the limit is shown in the CMSSM $m_0/m_{1/2}$ plane for ($\tan\beta = 50$, $A_0 = 0$, sgnμ = +).

Figure 15 shows the same result as a function of the physical masses for two benchmark simplified models [24–26]: gluino-LSP production (left) and squark-LSP production (right). The former refers to pair-produced gluinos, where each gluino directly decays to two light quarks and the LSP resulting in a four jet plus missing transverse energy final state and the latter to pair-produced squarks, where each squark decays to one jet and the LSP resulting in a two jet plus missing transverse energy final state.

8 Conclusion

A search for gluinos and scalar quarks is performed in a data sample of 35 pb^{-1} of pp collisions at $\sqrt{s}$ = 7 TeV, recorded by the CMS detector at the CERN LHC. The final state with large R and M_R is used in inclusive final state topologies. The search proceeds after the predictions of the Standard Model backgrounds have been calculated in data samples dominated by Standard Model processes. No significant excess over the background expectations is observed; The upper limit on signal events is calculated using a flat Bayesian prior for the signal and a log-normal prior for the background. For comparison the limits are also calculated using the reference prior technique. The results are presented in the m_0-$m_{1/2}$ CMSSM parameter space. For simplified models the result is given as a function of the gluino, squark and LSP masses.

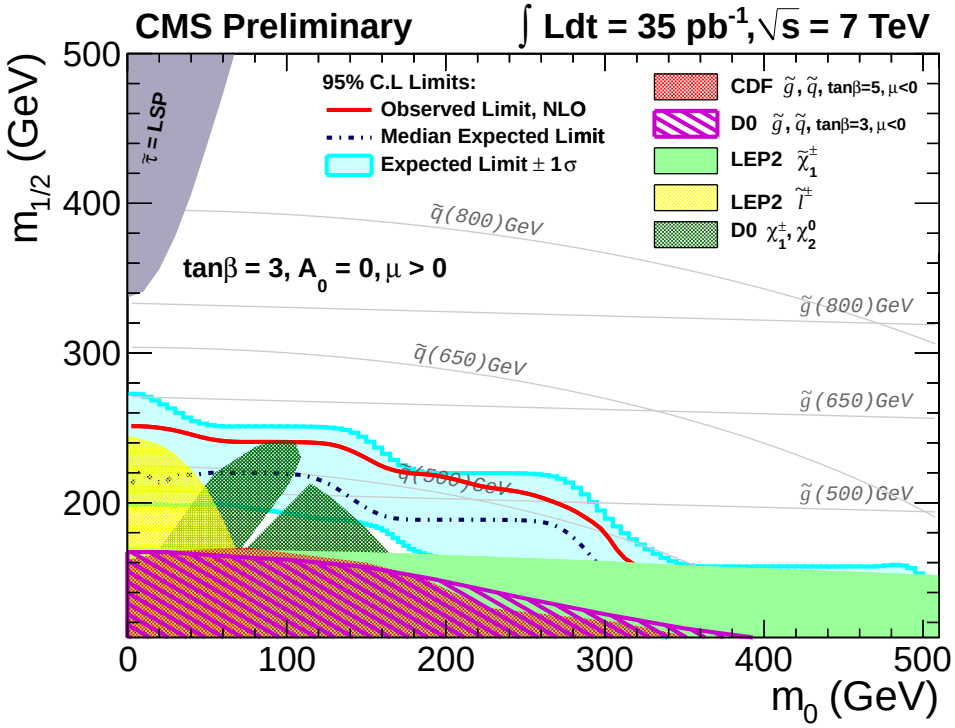

Figure 7: Limits on the CMSSM ($\tan\beta = 3$, $A_0 = 0$, sgnμ = +) in the $m_0/m_{1/2}$ plane for the ELE Box selection ($R > 0.45$, $M_R > 500$ GeV).

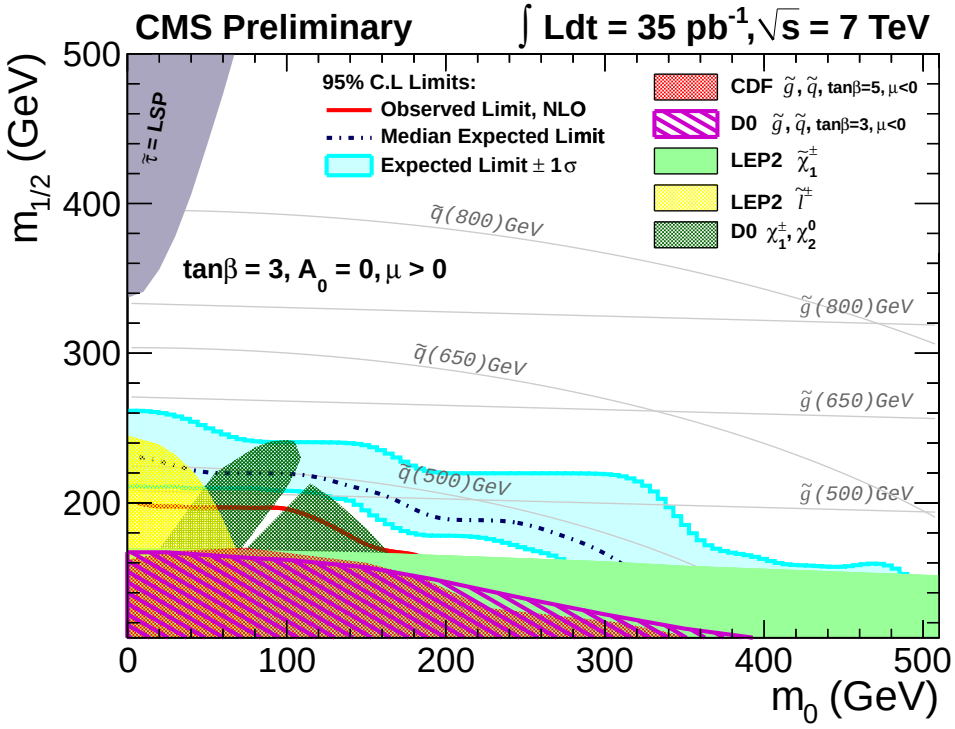

Figure 8: Limits on the CMSSM ($\tan\beta = 3$, $A_0 = 0$, sgnμ = +) in the $m_0/m_{1/2}$ plane for the MU Box selection ($R > 0.45$, $M_R > 500$ GeV).

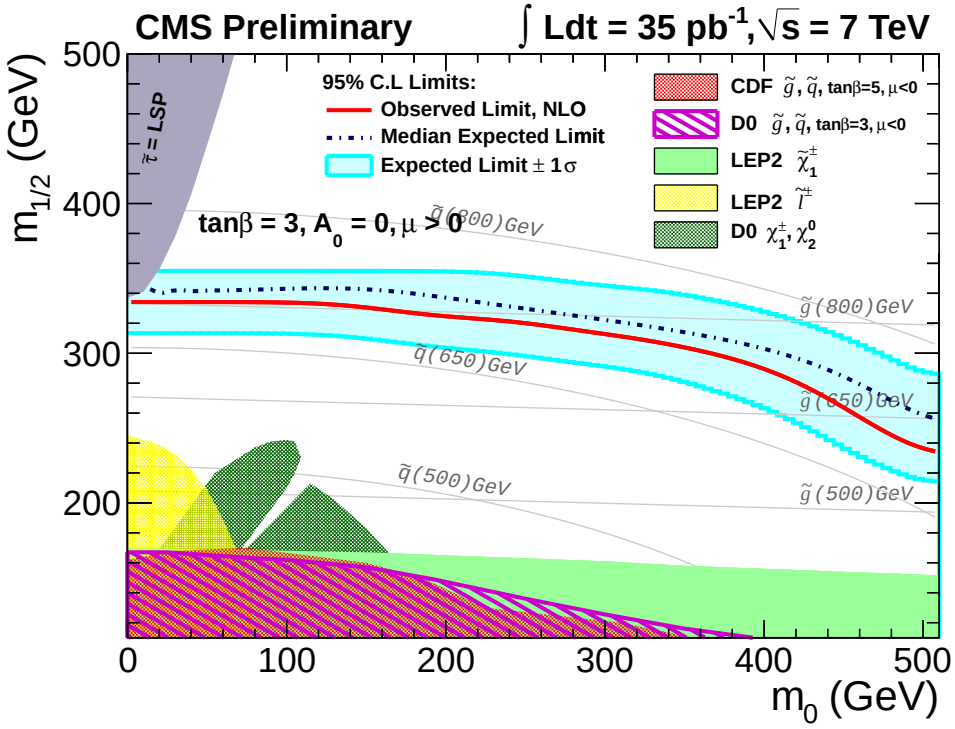

Figure 9: Limits on the CMSSM ($\tan\beta = 3$, $A_0 = 0$, sgnμ = +) in the $m_0/m_{1/2}$ plane for the HAD Box selection ($R > 0.5$, $M_R > 500$ GeV).

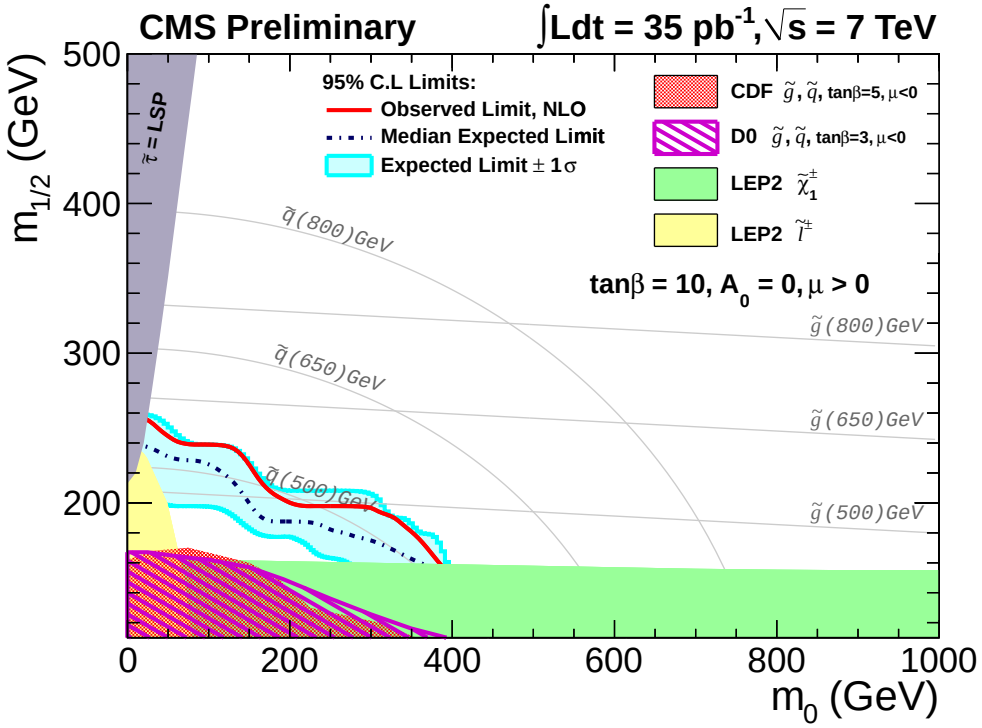

Figure 10: Limits on the CMSSM ($\tan\beta = 10$, $A_0 = 0$, sgnμ = +) in the $m_0/m_{1/2}$ plane for the ELE Box selection ($R > 0.45$, $M_R > 500$ GeV).

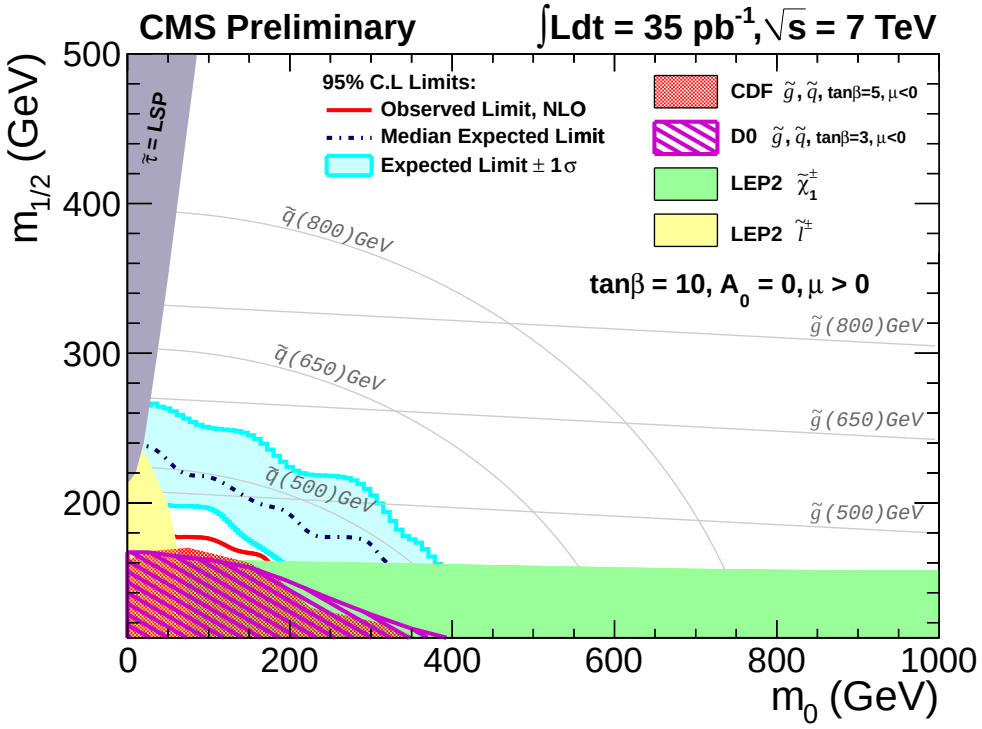

Figure 11: Limits on the CMSSM ($\tan\beta = 10$, $A_0 = 0$, sgnμ = +) in the $m_0/m_{1/2}$ plane for the MU Box selection ($R > 0.45$, $M_R > 500$ GeV).

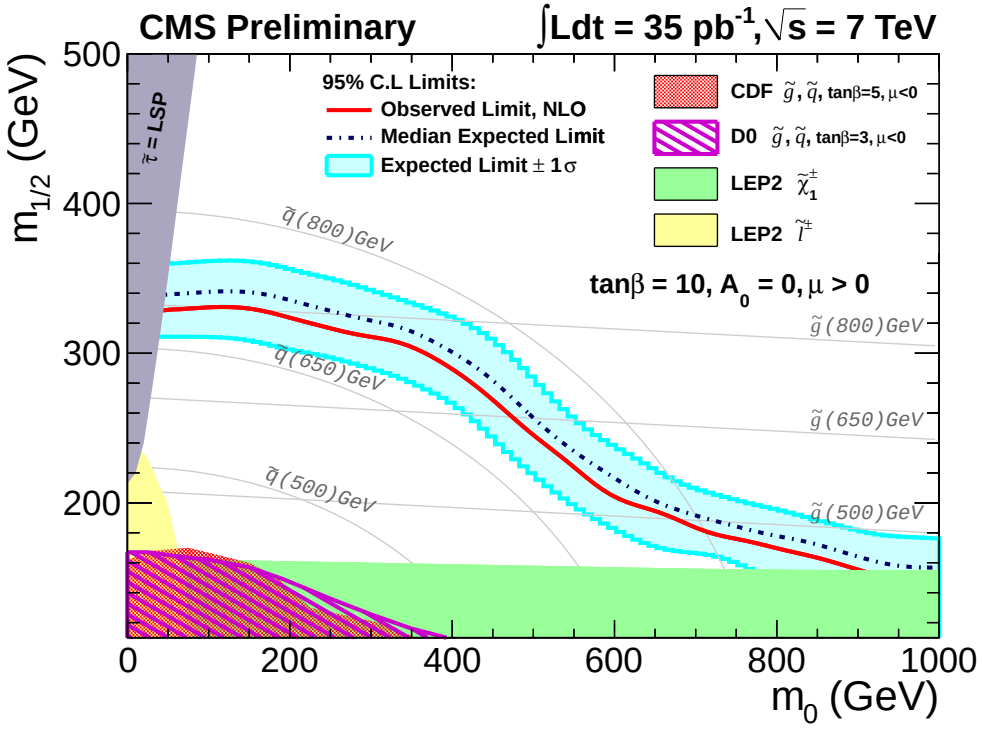

Figure 12: Limits on the CMSSM ($\tan\beta = 10$, $A_0 = 0$, sgnμ = +) in the $m_0/m_{1/2}$ plane for the HAD Box selection ($R > 0.5$, $M_R > 500$ GeV).

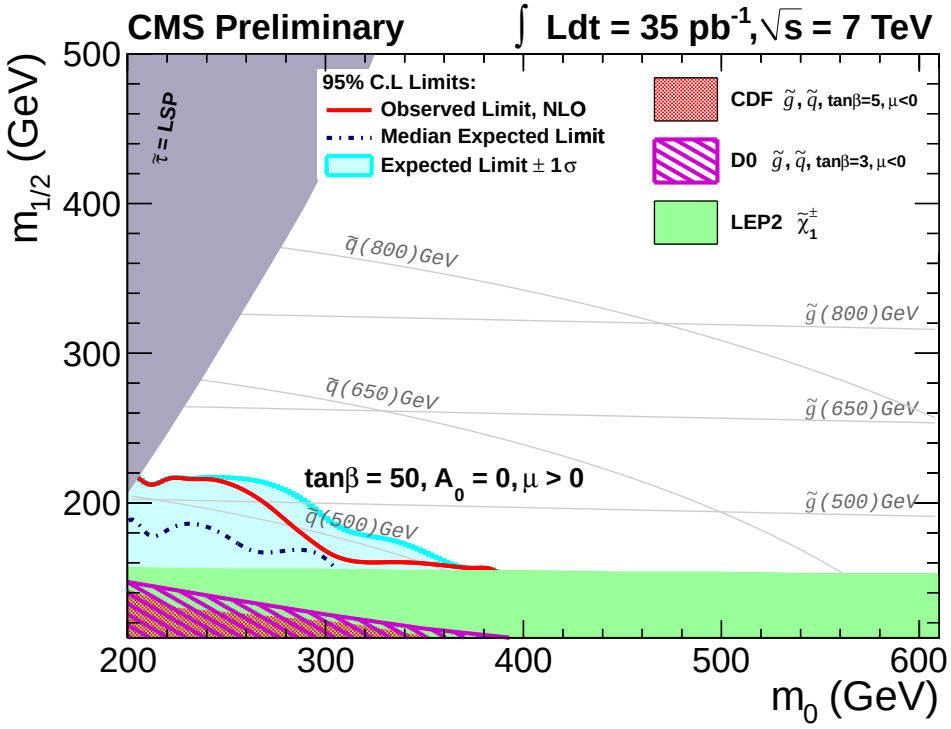

Figure 13: Limits on the CMSSM ($\tan\beta = 50$, $A_0 = 0$, sgnμ = +) in the $m_0/m_{1/2}$ plane for the ELE Box selection ($R > 0.45$, $M_R > 500$ GeV).

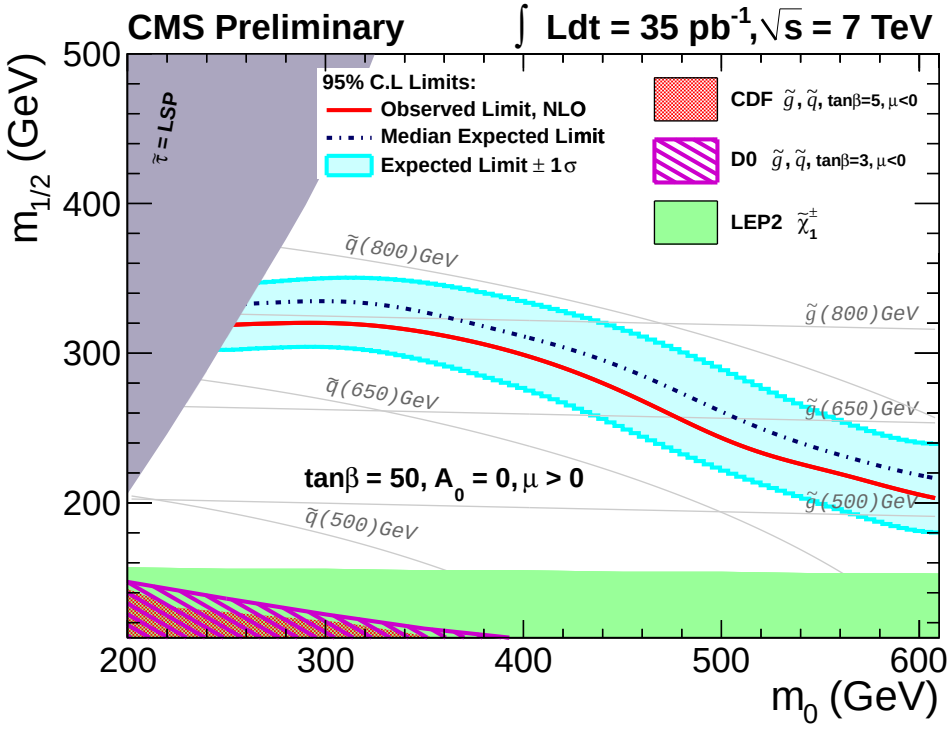

Figure 14: Limits on the CMSSM ($\tan\beta = 50$, $A_0 = 0$, sgnμ = +) in the $m_0/m_{1/2}$ plane for the HAD Box selection ($R > 0.5$, $M_R > 500$ GeV).

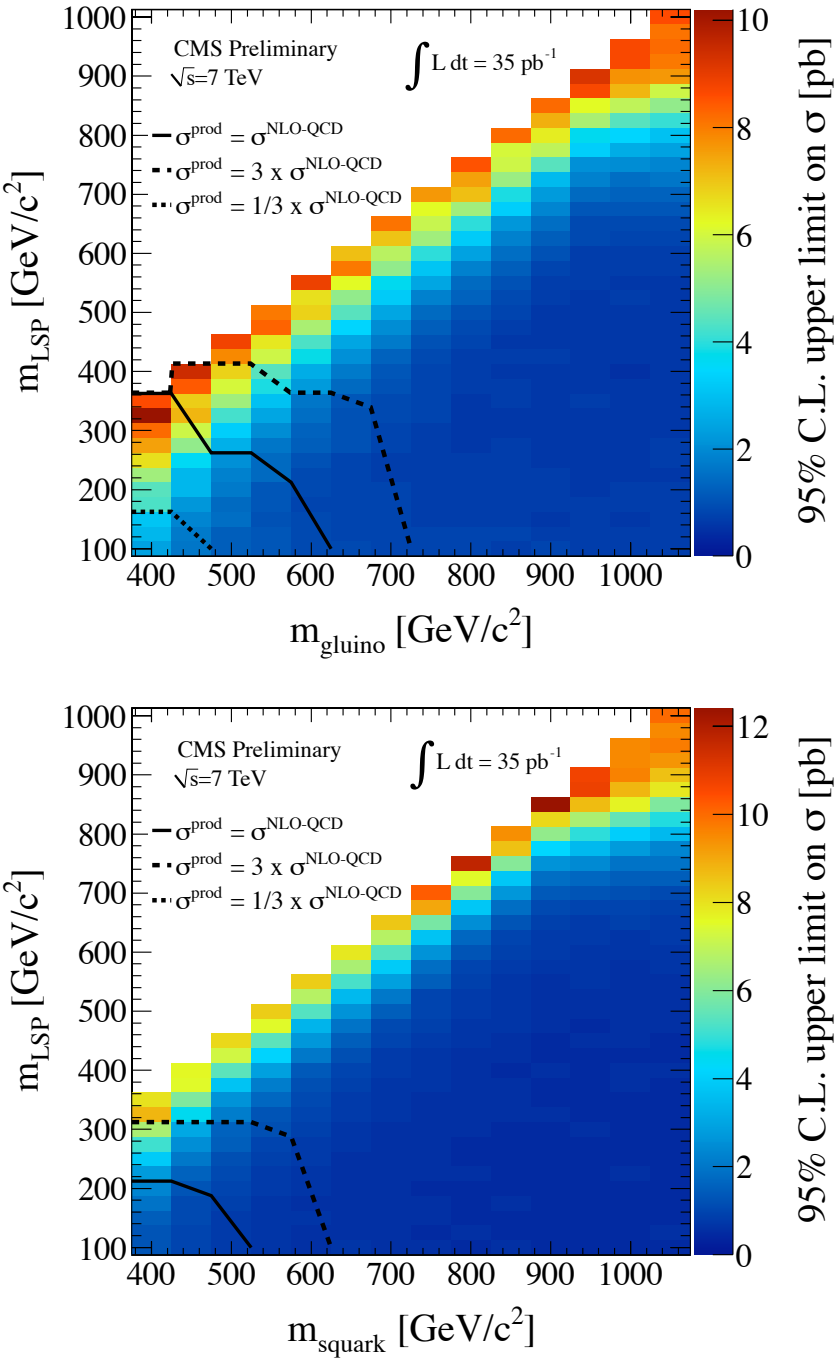

Figure 15: Limits on simplified models. (upper) di-gluino production resulting in a 4-jet + E_T^{miss} final state. (lower) di-squark production resulting in a 2-jet + E_T^{miss} final state. The z-axis (color scale) indicates the excluded at 95% C.L. cross section for each value of m_{LSP} and $m_{\mathrm{gluino}}/m_{\mathrm{squark}}$.

References

[1] P. Ramond, "Dual Theory for Free Fermions", *Phys. Rev.* **D3** (1971) 2415–2418. doi:10.1103/PhysRevD.3.2415.

[2] Y. Golfand and E. Likhtman, "Extension of the Algebra of Poincare Group Generators and Violation of p Invariance", *JETP Lett.* **13** (1971) 323–326.

[3] D. Volkov and V. Akulov, "Possible universal neutrino interaction", *JETP Lett.* **16** (1972) 438–440.

[4] J. Wess and B. Zumino, "Supergauge Transformations in Four-Dimensions", *Nucl. Phys.* **B70** (1974) 39–50. doi:10.1016/0550-3213(74)90355-1.

[5] P. Fayet, "Supergauge Invariant Extension of the Higgs Mechanism and a Model for the electron and Its Neutrino", *Nucl.Phys.* **B90** (1975) 104–124. doi:10.1016/0550-3213(75)90636-7.

[6] C. Rogan, "Kinematics for new dynamics at the LHC", arXiv:1006.2727.

[7] CMS Collaboration, "The CMS experiment at the CERN LHC", *JINST* **3** (2008) S08004. doi:10.1088/1748-0221/3/08/S08004.

[8] CMS Collaboration, "CMS technical design report, volume II: Physics performance", *J. Phys.* **G34** (2007) 995–1579. doi:10.1088/0954-3899/34/6/S01.

[9] CMS Collaboration, "Tracking and Primary Vertex Results in First 7 TeV Collisions", *CMS PAS* **TRK-10-005** (2010).

[10] M. Cacciari, G. P. Salam, and G. Soyez, "The anti-kt jet clustering algorithm", *JHEP* **0804:063** (2008). doi:10.1088/1126-6708/2008/04/063.

[11] CMS Collaboration, "Determination of the Jet Energy Scale in CMS with pp Collisions at sqrt(s) = 7 TeV", *CMS PAS* **JME-10-010** (2010).

[12] CMS Collaboration, "Commissioning of the Particle-Flow Reconstruction in Minimum-Bias and Jet Events from pp Collisions at 7 TeV", *CMS PAS* **PFT-10-002** (2010).

[13] CMS Collaboration, "Measurements of Inclusive W and Z Cross Sections in pp Collisions at 7 TeV", *CMS PAS* **EWK-10-002** (2010).

[14] A. H. Chamseddine, R. L. Arnowitt, and P. Nath, "Locally Supersymmetric Grand Unification", *Phys.Rev.Lett.* **49** (1982) 970. doi:10.1103/PhysRevLett.49.970.

[15] R. Barbieri, "Looking Beyond the Standard Model: The Supersymmetric Option", *Riv. Nuovo Cim.* **11N4** (1988) 1–45.

[16] L. J. Hall, J. D. Lykken, and S. Weinberg, "Supergravity as the Messenger of Supersymmetry Breaking", *Phys. Rev.* **D27** (1983) 2359–2378. doi:10.1103/PhysRevD.27.2359.

[17] G. L. Kane, C. F. Kolda, L. Roszkowski et al., "Study of constrained minimal supersymmetry", *Phys.Rev.* **D49** (1994) 6173–6210, arXiv:hep-ph/9312272. doi:10.1103/PhysRevD.49.6173.

[18] CMS Collaboration, "HCAL performance from first collisions data", *CMS Detector Performance Summary* **DPS-2010/025** (2010).

[19] CMS Collaboration, "Electromagnetic calorimeter commissioning and first results with 7 TeV data", *CMS Note* **2010/012** (2010).

[20] CMS Collaboration, "Selection of Top-Like Events in the Dilepton and Lepton-plus-Jets Channels in Early 7 TeV Data", *CMS PAS* **TOP-10-004** (2010).

[21] L. Demortier, S. Jain, and H. B. Prosper, "Reference priors for high energy physics", *Phys. Rev.* **D82** (2010) 034002, arXiv:1002.1111. doi:10.1103/PhysRevD.82.034002.

[22] D. Bourilkov, R. C. Group, and M. R. Whalley, "LHAPDF: PDF use from the Tevatron to the LHC", arXiv:hep-ph/0605240.

[23] CMS Collaboration, "Absolute luminosity normalization", *CMS DPS* **CERN-CMS-DP-2011-002** (2011).

[24] J. Alwall, P. Schuster, and N. Toro, "Simplified Models for a First Characterization of New Physics at the LHC", *Phys.Rev.* **D79** (2009) 075020, arXiv:0810.3921. doi:10.1103/PhysRevD.79.075020.

[25] J. Alwall, M. P. Le, M. Lisanti et al., "Searching for gluinos at the Tevatron and beyond", *Int.J.Mod.Phys.* **A23** (2008) 4637–4646. doi:10.1142/S0217751X0804281X.

[26] D. Alves et al., "Simplified Models for LHC New Physics Searches", *(to appear)* **lhcnewphysics.org** (2011).